PERGAMON International Journal of Mechanical Sciences 42 (2000) 1069–1086

International Journal of MECHANICAL SCIENCES

www.elsevier.com/locate/ijmecsci

Finite element analysis of the effect of sequential cuts and tool–chip friction on residual stresses in a machined layer

C.R. Liu, Y.B. Guo*

School of Industrial Engineering, Purdue University, West Lafayette, IN 47907, USA

Received 2 October 1998; received in revised form 7 April 1999

Abstract

A thermo-elastic–viscoplastic model using explicit finite element code Abaqus was developed to investigate the effect of sequential cuts and tool–chip friction on residual stresses in a machined layer. Chip formation, cutting forces and temperature were also examined in the sequential cuts. The affected layer from the first cut slightly changes the chip thickness, cutting forces, residual strain and temperature of the machined layer, but significantly affects the residual stress distribution produced by the second cut. Residual stress is sensitive to friction condition of the tool–chip interface. Simulation results offer an insight into residual stresses induced in sequential cuts. Based on simulation results, characteristics of residual stress distribution can be controlled by optimizing the second cut.

Keywords: Residual stress; Surface integrity; Finite element analysis; Metal cutting

1. Introduction

The quality of a mechanical component such as its geometrical stability and fatigue life are significantly affected by the surface integrity of the sublayer generated by the machining process. Surface integrity generally can be determined in terms of mechanical, metallurgical, chemical, and topological states. Residual stress is a major part of the mechanical state of a machined layer. It is generally believed that residual stresses result from plastic deformation, thermal stress, and phase transformation of the machined layer. Residual stresses in high performance alloys and steels are of

* Corresponding author.
E-mail addresses: liuch@ecn.purdue.edu (C.R. Liu), yuebin@ecn.purdue.edu (Y.B. Guo)

0020-7403/00/$ - see front matter
PII: S0020-7403(99)00042-9

Nomenclature

σ	total elastic stress
$\bar{\sigma}$	flow stress
σ_0	static yield stress
H	strength coefficient
n	strain hardening exponent
D^{el}	elasticity matrix
ε^{el}	total elastic strain
$\bar{\varepsilon}^{pl}$	effective plastic strain
$\dot{\bar{\varepsilon}}^{pl}$	effective plastic strain rate
$\bar{\varepsilon}_0^{pl}$	critical effective plastic strain
$\bar{\varepsilon}_f^{pl}$	failure effective plastic strain
T	temperature
c_i	material constants
D	material parameter
p	material parameter
∇T	temperature increment
f_1	work-to-heat conversion factor
f_2	conversion efficiency factor
ρ	density
C_p	specific heat
τ	friction shear stress
μ	friction coefficient
F_c	cutting force
F_t	thrust force
α	tool rake angle
c	coefficient
i	increment number
$\mathbf{U}$	displacement vector
Δt	time increment
$\mathbf{M}$	diagonal lumped mass matrix
F	applied load vector
I	internal force vector
S_{11}	normal residual stress in cutting direction

considerable industrial importance because they can affect failure by fatigue, creep or cracking. As flexibility and efficiency are becoming more and more important, superfinish hard turning was proposed to replace abrasion-based superfinishing (or AB superfinishing) in terms of residual stress and surface finish requirements [1]. A stumbling block to industrial application of hard turning

technology can be attributed partly to uncertainty about the residual stress induced in hard machining [1,2].

The bulk of the existing work on the surface integrity of the machined layer has been limited to experimental studies. Liu and Barash [3,4] found three quantitative measures to define the mechanical state of a machined layer. They also found that the effect of linear thermal expansion in the machined layer on residual stress distribution is negligible. In case of flank wear, the residual stress pattern is lightly or severely modified by temperature generated depending upon the cutting speed. Liu and Barash [5] showed that mechanical deformation of the workpiece surface is the one of the causes of producing both tensile and compressive residual stresses in machining. Kono et al. [6] presented findings that residual stress increases with the cutting speed, but does not monotonically change with the depth of cut in hard turning. These results contradict those from machining soft steel [7]. Schreiber and Schlicht [8] confirmed that the mechanical properties of the workpiece material to be machined have a great influence on the magnitude and distribution of the residual stresses. Matsumoto et al. [9] and Wu and Matsumoto [10] concluded that material hardness has a significant effect on the pattern of residual stress that remains in the machined part. Konig et al. [2] indicated that residual tensile stress is attributable to wear land friction, and the development of residual tensile stress depends primarily on the extent of wear land in turning 16 MnCr5 case hardened steel. Tonshoff et al. [11] found that the residual stresses were influenced by both the cutting speed and the tool wear because increasing the cutting speed will accelerate the tool wear. Liu and Mittal [1] proposed single step superfinishing hard turning for producing super surface integrity in terms of residual stress and surface finish.

Development of an analytical model of residual stress in metal cutting has been slow due to the inherent complexity of machining processes. Okushima and Kakino [12] considered the ploughing forces and the temperature distribution as the main causes of residual stresses. However, the calculated results did not agree well with the experimental results. Wu and Matsumoto [10] proposed a closed form solution to study the effect of workpiece hardness on the pattern of residual stresses in orthogonal cutting. Their results showed an agreement with the experimental data trends.

The finite element method has been widely used since 1980s for performing stress analysis in metal cutting. Several finite element models have been developed to predict residual stress using cutting forces and temperature from experiments and/or analytical solution as applied loads without chip formation by Lajczok [13], Natarajan and Jeelani [14], and Liu et al. [15,16]. Strenkowski and Carroll [17] used an effective plastic strain criterion for chip separation. The effective plastic strain criterion is the main factor to control the residual strain and residual stresses in the machined layer. Lin et al. [18,19] applied a strain energy density criterion to predict residual stress in machining. The FEM model by Shin [20] showed that the effects of thermal stresses and the cutting and clamping forces on the final distribution of residual stresses were important to the accurate prediction of residual stresses. The FEM results of Obikawa et al. [21] showed that residual stress induced in the continuous chip formation is greater than that in the discontinuous chip formation. However, several important factors (such as effects of temperature, strain rate, and force unloading) that influence residual stress were neglected. Residual stresses in drilling 304 stainless steel were demonstrated by finite element analysis by Guo and Dornfeld [22], but the residual stress was not a major concern of this research.

A literature review of residual stress in machining has shown that few practical models to predict the effect of sequential cuts on residual stress distribution in the machined layer have been reported. However, the affected layer by previous cutting is usually cut again in metal cutting process. It has been proposed in the metal cutting literature that the machining process is not unique and the residual stress will be affected by the previous cut because the newly generated surface layer has residual stress and strain, and it is also strain hardened. Further, a methodology to control the residual stress and its sensitivity to friction condition of the tool–chip interface has not been addressed. Theoretical analysis of residual stress formation is a challenging problem. In general, closed form analytical solutions for general elastic–plastic problems with large deformation, high strain and strain rate, and high-temperature coupling are very difficult to derive. Thus, finite element method is a feasible approach for modeling residual stresses in metal cutting. To solve these problems, an explicit dynamic FEM software package, ABAQUS/Explicit [23], was used in this study. The method has some important advantages for modeling metal cutting processes: (1) It is computationally efficient for the analysis of large models with relatively short dynamic response times and for the analysis of extremely discontinuous events or processes. (2) It can be used to perform analysis with complicated contact conditions. Contact algorithms are robust and straightforward than their implicit counterparts. Explicit are therefore attractive for problems such as metal cutting which involve complicated contact situations. (3) It uses a consistent, large-deformation theory models can undergo large rotation and large deformation which occurs in metal cutting. (4) It can be used to perform an adiabatic stress analysis if inelastic dissipation is expected to generate heat in the material. Adiabatic analysis is typically used to simulate high-speed manufacturing processes involving large amount of inelastic strain, where the heating of the material properties caused by its deformation is an important effect because of temperature-dependent material properties. (5) It allows for either automatic or fixed time increment. These features of explicit dynamics procedure make it ideally suitable for analyzing the residual stress in metal cutting.

2. Finite element modeling and assumptions

The two-dimensional finite element model, Fig. 1, was developed under the plane strain assumption that the width of the cut is at least five times greater than the uncut chip thickness. The length of edge BC is 20 times longer than that of the uncut chip thickness for assuring steady-state cutting. The workpiece is assumed to be semi-infinite in size compared to the cutting tool. This is accomplished by using semi-infinite elements at the bottom of the workpiece. The element type used in the other part of the workpiece is a four-node bilinear and reduced integration with hourglass control to deal with the large deformation caused by chip formation process. Note that some elements in the mesh are longer in the horizontal direction. This is done in anticipation of the intense compression and shear straining to be expected as the tool moves from right to left. By selecting this shape, numerical problem results from severe element distortion may be avoided. In this model, edge AB is constrained against displacement, and other edges are not constrained to allow deformation. For simplicity, a perfectly rigid cutting tool is assumed in view of the significantly high elastic moduli of most tool materials. This is also an acceptable approximation since the elastic deflection of the cutting tool is insignificant relative to the large plastic deformation

Table 1
Cutting tool geometry and cutting conditions

Rake angle	15°
Clearance angle	5°
Cutting speed	3 m/s
Uncut chip thickness	0.25 mm
Initial temperature	25°C

of the workpiece. A sharp cutting tool was modeled using rigid elements. The cutting tool is free to move in 1 direction. The boundary condition is enforced to constrain the motion of the cutting tool in two direction. The perfect cutting tool has friction capability to model the sticking and sliding interaction of the tool–chip which allows formation of the second shear zone as the tool advances through the workpiece.

A critical problem of simulating the effect of cutting sequence on residual stress is how to keep the physical state from the first cut and use it as initial condition of the second cut. In this study the physical state (all residual stress and strain components) of the machined surface after unloading in the first cut was used as initial conditions for the second cut. Other cutting conditions of the second cut are the same as those of the first cut. In order to predict residual stress, three unloading steps were implemented at the end of each cut in this study: (1) releasing the cutting forces, (2) releasing the clamping forces, and (3) cooling of the workpiece to room temperature.

The geometry of the cutting tool modeled and cutting conditions are given in Table 1. Residual stresses from phase transformation and cutting tool wear were neglected. The workpiece is assumed to be residual stresses free before the first cut. In addition, continuous chip formation was assumed in this study.

3. Governing equations and numerical solution

In this analysis, the workpiece material is 304 stainless steel. The thermo-elastic–plastic material properties of 304SS in Table 2 were used in this model [24,25]. The constitutive equations of the workpiece material are described below.

3.1. Flow stress

In order to quantify the effect of plastic flow characteristics of the workpiece material on the cutting process, a thermo-elastic–plastic model with isotropic hardening and strain rate dependence was considered in the analysis. In the linear elasticity regime, the total stress is defined from the total elastic strain as [23]

$$\sigma = D^{el}\varepsilon^{el}, \tag{1}$$

Table 2
Material properties of annealed 304 stainless steel

Density	7800 kg/m^3	Young's modulus (Gpa, °C)	(193, 25)
Strain-rate dependent	$D = 1500$, $p = 6$		(179, 260)
Inelastic heat fraction	0.9		(160, 480)
			(140, 700)
Specific heat	(450, 25)		
(J/kg, °C)	(500, 100)	Yield and fracture strength,	(230, 0, 25)
	(525, 450)	fracture strain and temperature	(554, 1.6, 25)
	(550, 850)	(Mpa, °C)	(154, 0, 426)
			(430, 1.19, 426)
Poisson's ratio (, °C)	(0.3, 25)		(146, 0, 537)
	(0.3, 260)		(390, 1.35, 537)
	(0.28, 480)		(96, 0, 648)
	(0.28, 700)		(289, 0.77, 648)

where σ is the total elastic stress, D^{el} is the elasticity matrix, and ε^{el} is the total elastic strain. D^{el} is defined by giving Young's modulus and Poisson's ratio, Table 2. These parameters are given as functions of temperatures.

In the plastic regime, flow stress may be expressed in the form

$$\bar{\sigma} = f(\bar{\varepsilon}^{pl}, \dot{\bar{\varepsilon}}^{pl}, T, c1, c2, \dots), \tag{2}$$

where ε^{pl}, $\dot{\bar{\varepsilon}}^{pl}$ are effective plastic strain and effective plastic strain rate, respectively, T is the temperature, and $c1$ and $c2$ are material constants. Flow stress with strain hardening may be expressed as

$$\bar{\sigma} = H\bar{\varepsilon}^{pl^n} \quad \text{for } \bar{\varepsilon}^{pl} \leqslant \varepsilon_c, \tag{3}$$

where $\bar{\sigma}$ is the flow stress, H is the strength coefficient, n is the strain hardening exponent, $\bar{\varepsilon}^{pl}$ is the effective plastic strain, and ε_c is the critical effective strain. In this study, the material strain hardening was modeled by defining flow stresses as a function of plastic strain and temperature, Table 2. The values of H and n were determined from these input values.

3.2. Strain rate

The work material deforms extensively along the shear plane as it flows through this zone. Considering high strain rate in metal cutting is essential because of its effects on the strength of the material. For many alloy steels this effect becomes very important in metal cutting. The strain rate is represented by over stress power law

$$\dot{\bar{\varepsilon}}^{pl} = D\left(\frac{\bar{\sigma}}{\sigma_0} - 1\right)^p \quad \text{for } \bar{\sigma} \geqslant \sigma_0, \tag{4}$$

where $\dot{\bar{\varepsilon}}^{pl}$ is the equivalent plastic strain rate, $\bar{\sigma}$ is the effective yield stress at a nonzero strain rate, σ_0 is the static yield stress (zero strain rate), and D, p are material parameters that may be functions

of temperature. These parameters are indicative of the strain rate sensitivity and can be determined from experiments as 1500 and 6, respectively [25].

3.3. Heat generation

Heat generation during metal cutting is important in tool wear and plays an important role in surface integrity and chip formation. The majority of the heat generated in the metal cutting process comes from plastic deformation and chip tool interface friction. High-temperatures and large-temperature gradient in metal cutting causes strength reduction of the workpiece material. The ductile failure model used in this study also indicates this phenomenon.

As a first approximation, the heat generation incorporated in this study assumes adiabatic condition. The temperature increment associated with the heat generation may be expressed by

$$\nabla T = \frac{f_1 * f_2 * \bar{\sigma} * \partial \bar{\varepsilon}^{pl}}{\rho C_p}, \tag{5}$$

where ∇T is the temperature increment. f_1 is the work-to-heat conversion factor, f_2 is the conversion efficiency factor, both f_1 and f_2 were taken as 0.9 as most of the workpiece deformation is converted to thermal energy. $\bar{\sigma}$ is the effective stress and $\partial \bar{\varepsilon}^{pl}$ is the effective plastic strain increment, and ρ and C_p are the material density and specific heat, respectively.

3.4. Chip separation criterion

In the finite element analysis of metal cutting, two factors are important in choosing a chip separation criterion, i.e., the type of criterion and the magnitude of criterion. The type of criterion should be based on the physics of chip separation. The magnitude depends on properties of the work material under cutting conditions. A variety of chip separation criteria, either geometrical or physical variables, and associated magnitudes have been proposed to simulate metal cutting process. The physics of chip separation has not been clearly characterized because elements cannot be made small enough to simulate a dislocation. Further, a reliable procedure for determining the magnitude of the criterion is not available. Therefore, it is hard to determine which of these separation criteria is better. However, the magnitude of the chip separation criteria affects the chip separation process, the stress distributions in the machined layer, and the distributions of effective plastic strain both in the chip and the machined surface [26]. Effective plastic strain criterion [17] and strain energy density criterion [19] have been used to investigate residual stress distribution. Geometrical criterion has also been used to study residual stress [20,21]. The disadvantage of the geometrical criterion is that it has no physical meaning. A material ductile failure model based on effective plastic strain was used in this study. When the effective strain of the material reaches $\bar{\varepsilon}_0^{pl}$, the critical effective strain, damage in the material initiates. When the effective strain reaches $\bar{\varepsilon}_f^{pl}$, the failure effective strain, due to further deformation, the material fails and loses its ability to resist any further load. The metal plasticity model in this paper uses the Mises stress potential for isotropic behavior. However, the potential depends only on the deviatoric stress and is independent of hydrostatic stress instead of normal stress on the shear plane. The proposed fracture criterion does not take care of the microcracks in the free surface. Plastic deformation of the material assumes

no inhomogeneity due to microcrack formation. The ductile failure criterion, denoted as FC, is defined as

$$FC = (\bar{\varepsilon}_0^{pl}, \bar{\varepsilon}_f^{pl}). \tag{6}$$

This criterion applies to all elements that are potentially part of the chip which contact the cutting tool edge. The determination of values for $\bar{\varepsilon}_0^{pl}$ and $\bar{\varepsilon}_f^{pl}$ in steady-state cutting process has been derived based on cutting mechanics [22]. In this study, $\bar{\varepsilon}_f^{pl}$ and $\bar{\varepsilon}_0^{pl}$ were 0.85 and 0.8, respectively, from the experimental data.

3.5. Friction condition

The study of tool–chip interaction in finite element simulation concerns force transmission at the interface, and thus determines surface integrity of a machined layer. The key issue is the variation of frictional and normal stress on the rake face. Two distinct regions of sliding and sticking were observed on the rake face. Experimental results [27,28] exhibited a constant coefficient of friction in the region for frictional shear stress lower than certain value and an approximate constant frictional stress (shear flow stress) thereafter. Based on experimental stress distribution and direct observation of the rake face, a constant coefficient of friction is proposed in the sliding region and for dry friction conditions and an equivalent shear stress limit, $\bar{\tau}_{\max}$, in the sticking region for ideal seizure conditions as an approximation. Whether a contact point is sliding or sticking depends on the stress state at that point. Regardless of the magnitude of the contact pressure stress, sliding will occur if the magnitude of the equivalent shear stress reaches $\bar{\tau}_{\max}$. Mathematically, this can be stated as

$$\tau_{crit} = \mu\sigma \quad \text{when } \tau < \bar{\tau}_{\max}, \tag{7}$$

$$\tau = \bar{\tau}_{\max} \quad \text{when } \tau \geqslant \bar{\tau}_{\max}. \tag{8}$$

The Coulomb friction model defines the critical shear stress, τ_{crit}, at which sliding of the surfaces starts as a fraction of the contact pressure, σ, between the surfaces ($\tau_{crit} = \mu\sigma$). The shear stress limit is typically introduced in cases when the contact pressure stress may become very large (as can happen in some manufacturing processes such as metal cutting) causing the Coulomb theory to provide a critical shear stress at the interface that exceeds the yield stress in the material beneath the contact surface. An upper bound estimate for $\bar{\tau}_{\max}$ is $\sigma_y/\sqrt{3}$, which σ_y is the Mises yield stress of the material adjacent to the surface.

An ideal way to obtain the coefficient of friction in the sliding region is based on the data of the stress distribution on the rake and flank wear faces from machining test. However, on-line measurement of stress distribution in the faces in machining is a changeling. Alternatively, the mean coefficient of friction in the sliding zone will be calculated from measuring cutting and feed forces. In case of sharp tool, the mean coefficient of friction between tool–chip in orthogonal cutting may be calculated by

$$\mu = c\frac{F_t + F_c \tan\alpha}{F_c - F_t \tan\alpha}, \tag{9}$$

where F_c and F_t are measured cutting and thrust forces, α is rake angle, and c is a coefficient. The value of c depends on the difference between measured and simulated forces. If the difference is less than 5%, the friction coefficient can be considered acceptable because the variation in measuring cutting and thrust forces can be as high as 10–15%. Otherwise, a modified coefficient value will be used and the difference will be checked again. This process will continue until the acceptable calculated forces are obtained. The advantage of this proposed approach is that the data of measured cutting and thrust forces are relatively easy to obtain.

3.6. Equations of motion

The explicit dynamics analysis procedure is based on implementation of an explicit integration rule together with the use of diagonal or lumped element mass matrices. The equations of motion for the body are integrated using the explicit central difference integration rule [23]

$$\dot{u}^{(i+1/2)} = \dot{u}^{(i-1/2)} + \frac{\Delta t^{(i+1)} + \Delta t^{(i)}}{2}\ddot{u}^{(i)}, \tag{10}$$

$$u^{(i+1)} = u^{(i)} + \Delta t^{(i+1)}\dot{u}^{(i+1/2)}, \tag{11}$$

where the subscript (i) refers to the increment number, U represents the displacement vector and Δt represents the time increment. The central difference integration operator is explicit in that the kinematic state may be advanced using known values of $\dot{u}^{(i-1/2)}$ and $\ddot{u}^{(i)}$ from the previous increment. The explicit integration rule provides high computation efficiency due to the use of diagonal element mass matrices because the accelerations at the beginning of the increment may be computed by

$$\ddot{u}^{(i)} = M^{-1} \bullet (F^{(i)} - I^{(i)}), \tag{12}$$

where M is the diagonal lumped mass matrix, F is the applied load vector, and I is the internal force vector. The explicit procedure integrates through time by using many small time increments for assuring convergence.

4. Simulation results and discussion

4.1. Chip formation

Fig. 1 shows chip formation process in the sequential cuts. It is recognized that the steady-state cutting is obtained in the point of chip formation, cutting forces, and distributions of stress/strain. Chip morphology of the first cut is almost identical to that of the second cut except that thickness of the second chip is about 3% thinner, but the thickness difference is so small that it can be ignored. From calculation, the shear angle is 14.5° and 15.1° for the first and the second cut, respectively. The model suggests that the first cut produced work hardening in the workpiece that the second cut "sees". The effect of increased hardness on the onset shear plate is to increase the shear angle, so the model is reasonable. The increase in shear angle results in a thinner chip (large shear angle for the same uncut chip thickness) and large forces and less surface damage. This shows evidence that material properties have been modified by the first cut.

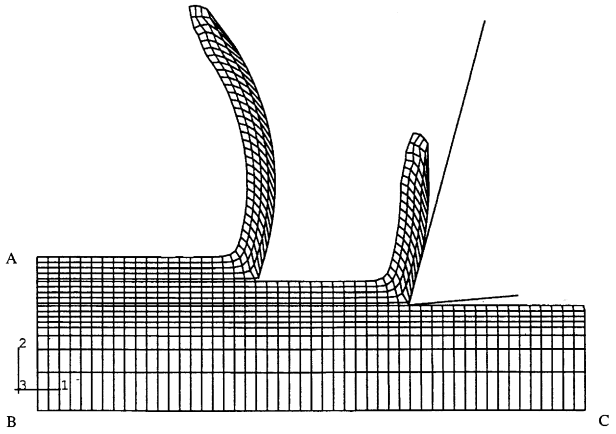

Fig. 1. Chip formation in subsequent cuts.

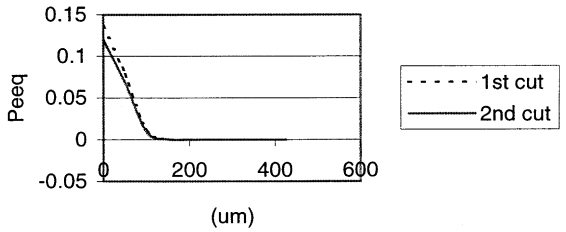

Fig. 2. Equivalent plastic strain (Peeq) distribution in vertical direction.

Fig. 2 shows the equivalent plastic strain distribution in the two direction. The equivalent plastic strain on the machined surface goes down from 0.14 to 0.12. Thus the degree of strain hardening near the machined surface from the first cut is larger than that from the second cut. The depth of affected layer may be expressed by the distance δ from the machined surface. δ_1 of 375 μm in the first machined layer is larger than δ_2 of 276 μm in the second machined layer. Therefore, the affected layer from the first cut is deep.

The influence of the strain hardened machined layer from the first cut is expected. It is partly responsible for the differences in shear angle and hence shear plane length, residual stress and strain distribution in the two cuts. Liu and Brash [3] found that there is a close correlation between the shear plane length and residual stress of the machined surface. The relationship of the affected layer and residual stress is not clear, However, it can be inferred that they are closely related if the second cut is within a certain depth of the affected layer with residual stress/strain and strain hardening from the first cut.

4.2. Cutting forces

The calculated cutting F_c and thrust force F_t are shown in Figs. 3 and 4. The difference between the calculated average forces and the measured forces are smaller than 5%. The measured forces to

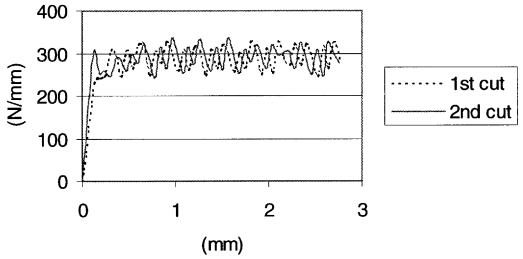

Fig. 3. Cutting force F_c.

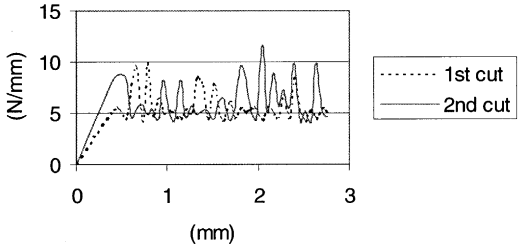

Fig. 4. Thrust force F_t.

determine the friction coefficient of tool–chip interface are not shown. No appreciable differences of calculated cutting and thrust forces exist between the two cuts in terms of magnitude and pattern. Steady-state cutting is assumed to be reached when the cutting forces approach steady-state values. Both cutting and thrust forces vary within certain amplitude due to node separation in cutting process. This variation is inherent in the finite element method. Compared to the average cutting forces, the average thrust forces are small because of the high rake angle of 15° used. In addition to cutting conditions, the values of cutting and thrust forces may also be affected by the plane strain assumption, which restricts material flow in the width direction of the chip. However, a negligible error exists because the ratio of the uncut chip thickness to the undeformed chip width is $\frac{1}{4000}$ in this study.

Cutting and thrust forces are generally unaffected by the separation criterion because they are calculated by averaging nodal forces over the entire rake face. The effect of the tool tip node is significantly lessened.

4.3. Residual stresses distribution

Residual stresses induced in the sequential cuts were investigated. Figs. 5 and 6 show the change of the distribution of residual normal stress S11 in the cutting direction of the two cuts. High tensile stresses are generated near the machined surface after the first cut, while the tensile residual stress is considerably changed after the second cut, and a compressive residual stress region near the machined surface is observed in Fig. 7. It is clear that the level of residual stress S11 decreases

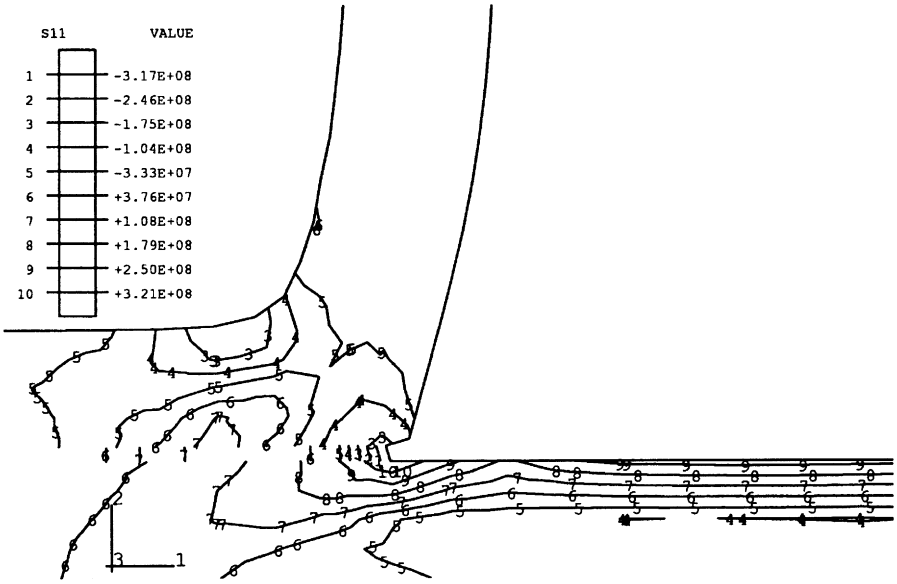

Fig. 5. Normal stress S11 (Pa) in horizontal direction in the first cut.

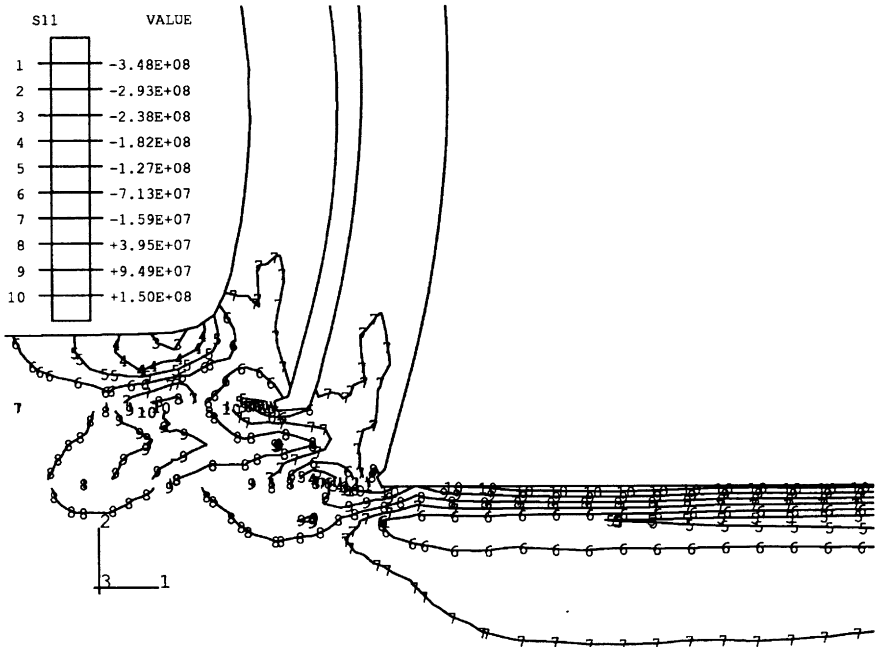

Fig. 6. Normal stress S11 (Pa) in horizontal direction in the second cut.

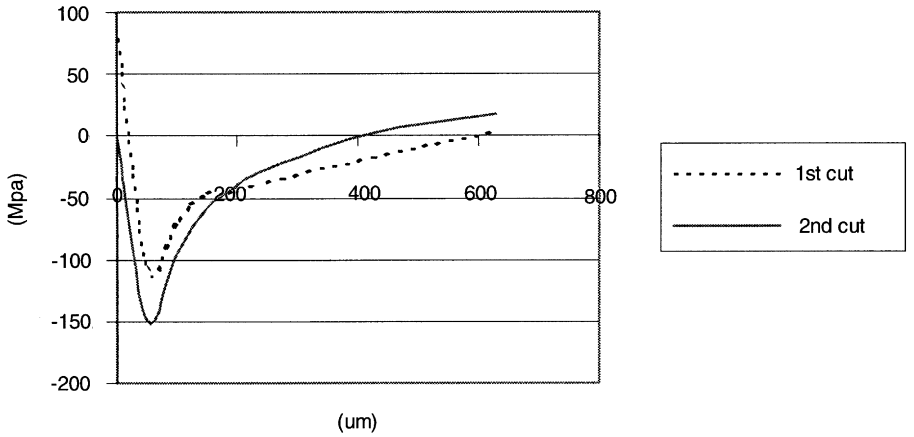

Fig. 7. Normal stress S11 distribution in vertical direction.

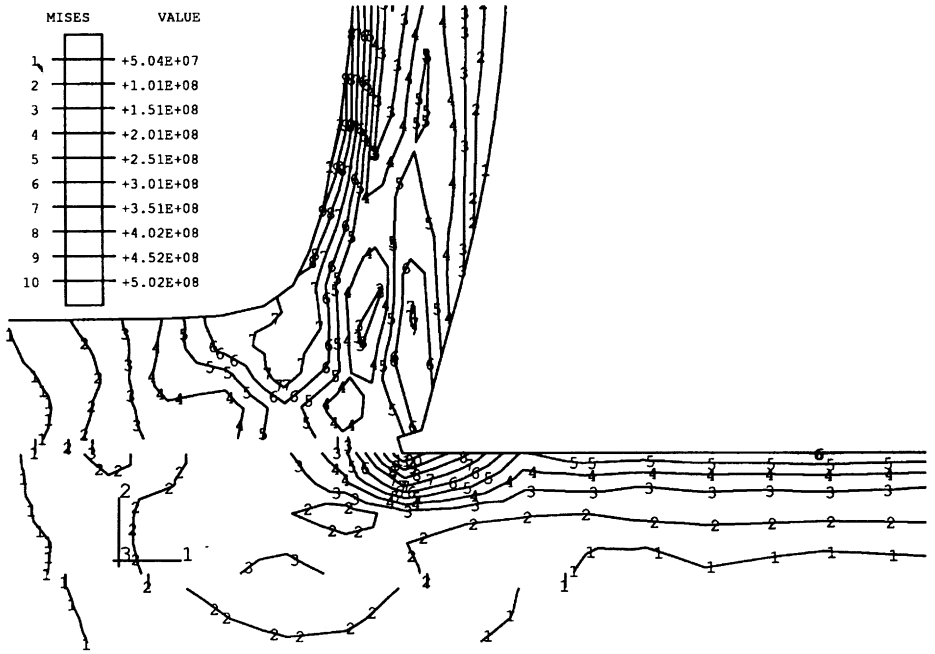

Fig. 8. Von Mises stress (Pa) in horizontal direction in first cut.

greatly after the second cut. Simulation result shows that the values of residual von Mises stress, Figs. 8 and 9, also decrease, but not as much as that of the residual normal stress S11.

Fig. 7 shows the distribution of S11 in the machined layer versus the depth from the machined surface in the two cuts. The high tensile stress layer left after the first cut is changed by the identical

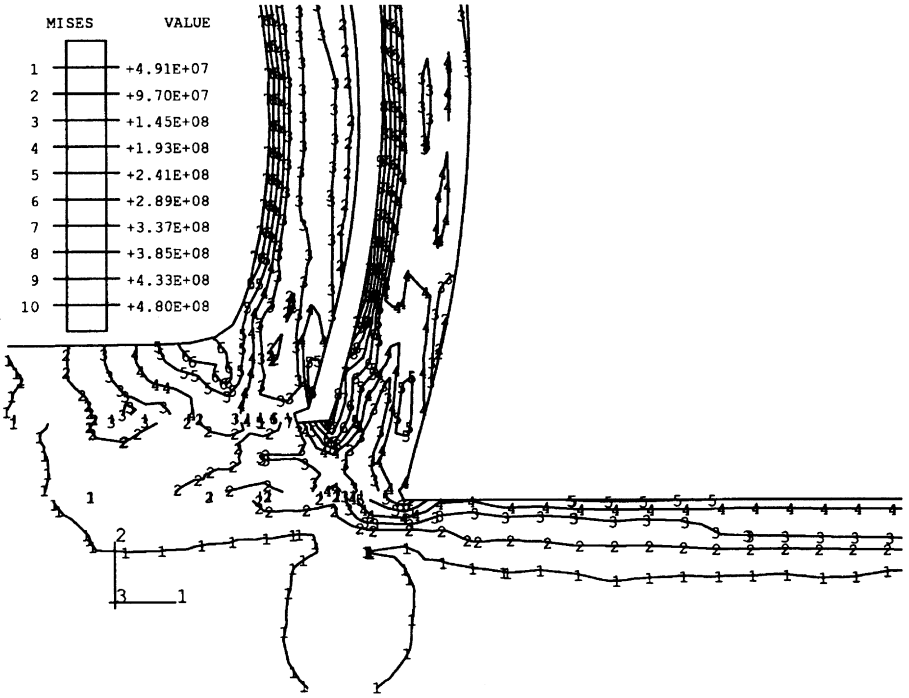

Fig. 9. Von Mises stress (Pa) in horizontal direction in the second cut.

second cut. The pattern of the stress distribution is modified. A compressive region exists just under the finished surface of the second cut, and the level of the compressive stress increases in the inner layer. Compressive residual stress S11 goes deep into the machined layer in the first cut. Thus, it indicates that residual stress S11 control in the machined layer is possible by optimizing the second cut. Experimental result [29] shows that residual stress S11 is tensile usually on the machined surface in the first cut in machining aluminum. That S11 may become compressive depends on the uncut chip thickness of the second cut. This provides indirect experimental evidence that the residual stress pattern follows the simulated pattern.

Compared to the cutting forces, all components of residual stress may be changed by the second cut. The magnitude of the residual stress usually increases with the value of the separation criterion because the separation criterion is applied only to the nodes closest to the tool tip. Therefore, caution must be exercised in selecting an appropriate value of the criterion to solve the residual stress problem. By constraining the nodes to remain fixed to the workpiece for a longer time, cutting forces are transmitted to the subsurface of the machined surface, resulting in the observed residual stress.

4.4. Residual stress sensitivity to friction condition of tool–chip interface

The average friction coefficient of tool–chip interface determined from the measured forces was used to study the effect of sequential cuts on residual stresses in the machined layer. However, the

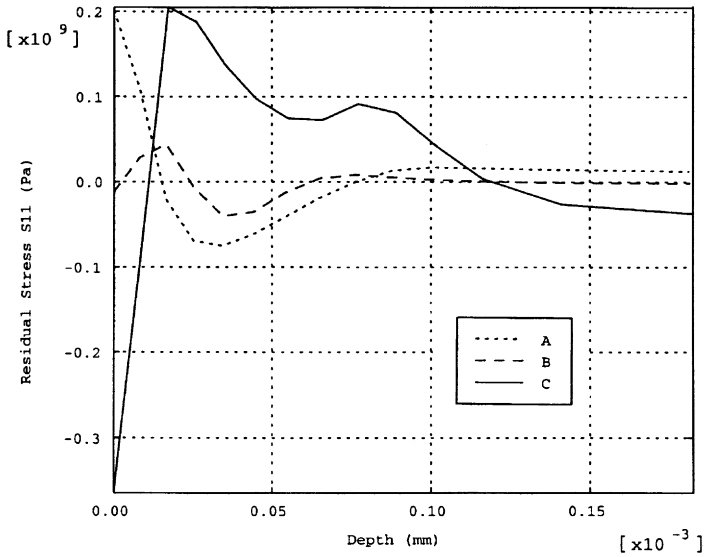

Fig. 10. Residual stress sensitivity to friction condition of tool–chip interface: A — 0.3; B — 0.5; C — 0.7.

friction coefficient of tool–chip interface is affected by both the tool rake angle and the coolant used, besides the influence of workpiece material. For the same tool rake angle and workpiece material, the friction coefficient may vary greatly, and thus the friction force applied to the workpiece. So residual stresses are expected to be affected by the friction force on the tool–chip interface. Considering the rake angle of 15° used in this study, the variation range of the friction coefficient is around 0.3–0.7 using different coolant in machining steels [30]. In order to investigate residual stress sensitivity to the friction condition, three levels of friction coefficient were selected to be 0.3, 0.5, and 0.7. For improving simulation accuracy, the finite element mesh was refined and the uncut chip thickness was assumed to be 0.1 mm. Other cutting conditions were same as those in Table 1. Fig. 10 shows residual stress S_{11} distribution under the three friction conditions. Residual stress S_{11} is tensile on the machined surface under low friction coefficient 0.3. As the friction coefficient value increases from 0.3 to 0.5, then 0.7, residual stress S_{11} changes from tensile to compressive on the machined surface. The residual stress distribution pattern also changes correspondingly.

4.5. Cutting temperature

Fig. 11 shows the temperature distribution of the chip–tool interface in the two cuts. They show that there is a friction heat source on the tool–chip interface as well as the heat source of plastic deformation. The highest chip–tool interface temperature resulting in crate wear is not located at the tip, but at a point along the rake face of the tool. The maximum temperature at the chip–tool interface is around 1050°C. The computed temperature may be slightly higher than that from the experiment due to the assumption of the adiabatic condition and no heat conduction occurs between the chip and the cutting tool. The temperature difference of the chip–tool interface at the

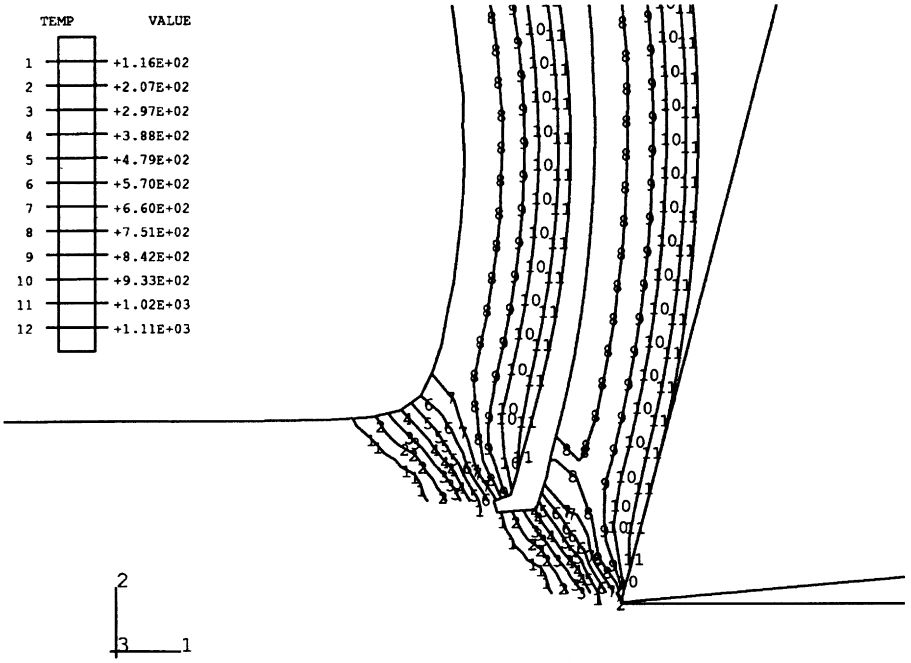

Fig. 11. Chip temperature distribution in the two cuts.

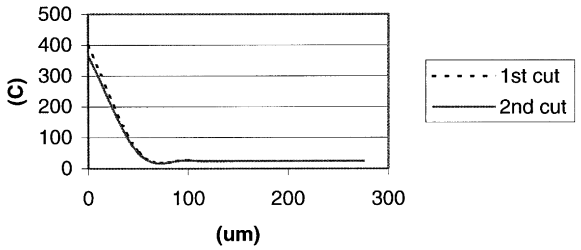

Fig. 12. Temperature distribution in the machined layer in vertical direction.

two cuts is negligible. However, Fig. 12 shows that the temperature of the machined surface after the second cut, 365.4°C, is slightly lower than that of the first cut, which is 398.7°C. Temperature gradients in the machined layer are high at both cuts. They affect only a very thin region below the machined surface. The temperature on the machined surface plays an important role in determining the residual stress distribution as temperature may affect the residual stresses distribution by inducing phase transformation and thermal expansion. It may also affect other aspects of surface integrity. From calculations, the maximum temperature on the machined surface is 398.7°C, which is lower than the phase transformation temperature for the material used in this study. Therefore, residual stress distribution might not be affected by phase transformation. This justifies the modeling assumption.

5. Conclusion

A thermo-elastic–plastic coupling FEM model was proposed to predict the effect of sequential cuts on the residual stress in the machined layer. The mechanical state from the first cut is used as the initial condition for the second cut.

Tensile residual stress on the machined surface in the first cut may be changed to compressive by optimizing the second cut. The levels of von Mises stress and hydrostatic stress are also reduced but not as much as that of normal stress in cutting direction. The region of the affected layer in the second cut becomes thinner. Changes of shear angle and chip thickness have all influence on residual stress/strain of the second cut. Residual stress on the machined surface is sensitive to the friction condition of the tool–chip interface.

Cutting forces, chip geometry, and temperature of the machined layer are only slightly affected by the sequential cuts. Temperature on the machined surface is below the phase transformation temperature.

Acknowledgements

This research has been supported by NSF under grant DMI-96102022, cost shared by USAF Manufacturing Technology program, Caterpillar Inc., Torrington Co., and Ford Motor Co.

References

[1] Liu CR, Mittal S. Single-step superfinish hard machining: feasibility and feasible cutting conditions. Journal of Robotics and Computer-Integrated Manufacturing 1996;12(1):15–27.

[2] Konig W, Berktold A, Koch KF. Turning versus grinding — a comparison of surface integrity aspects and attainable accuracy. Annals of the CIRP 1993;42(1):39–43.

[3] Liu CR, Barash MM. The mechanical state of the sublayer of a surface generated by chip-removal process, Part 1: cutting with a sharp tool. Transactions of the ASME, Journal of Engineering for Industry 1976a;November:1192–201.

[4] Liu CR, Barash MM. The mechanical state of the sublayer of a surface generated by chip-removal process, Part 2: cutting with a tool with flank wear. Transactions of the ASME, Journal of Engineering for Industry 1976b; November:1202–8.

[5] Liu CR, Barash MM. Variables governing patterns of mechanical residual stress in a machined surface. Transactions of the ASME, Journal of Engineering for Industry 1982;104(3):257–64.

[6] Kono Y, Hara A, Yazu S, Uchida T, Mori Y. Cutting performance of sintered CBN tools, Cutting tool materials. Proceedings of the International Conference, American Society for Metals, Ft. Mitchell, Kentucky, September 15–17, 1980, pp. 218–95.

[7] El-Khabeery MM, Fattouh M. Residual stresses distribution caused by milling. International Journal of Machine Tools Manufacture 1989;29(3):391–401.

[8] Schreiber E, Schlicht H. Residual stress after turning of hardened components. The International Conference On Residual Stresses. Garnish-Partenkirchen (FRG), 1986, 853–60.

[9] Matsumoto Y, Barash MM, Liu CR. Effects of hardness on the surface integrity of AISI 4340 steel. Transactions of the ASME, Journal of Engineering for Industry 1986;108:169–75.

[10] Wu DW, Matsumoto Y. The effect of hardness on residual stresses in orthogonal machining of AISI 4340 steel. Transactions of the ASME, Journal of Engineering for Industry 1990;112(3):245–52.

[11] Tonshoff HK, Wobker HG, Brandt D. Tribological aspects of hard turning with ceramic tools. Journal of the Society of Tribologists and Lubrication Engineers 1995;51(2):163–8.
[12] Okushima K, Kakino Y. The residual stresses produced by metal cutting. Annals of the CIRP 1971;10(1);13–4.
[13] Lajczok MR. A study of some aspects of metal machining using the finite element method. PhD Dissertation, North Carolina State University, 1980.
[14] Natarajan R, Jeelani S. Residual stresses in machining using finite element method. Computers in Engineering, Computer Software and Applications ASME, New York, 1983;3:19–20.
[15] Liu CR, Lin ZC, Barash MM. Effects of plane strain and plane stress conditions on stress filed in the workpiece during machining — an elasto-plastic finite element analysis. High Speed Machining 1984;2:167–80.
[16] Liu CR, Lin ZC, Barash MM. Thermal and mechanical stresses in the workpiece during machining. High Speed Machining 1984;2:181–91.
[17] Strenkowski JS, Carroll JT. A finite element model of orthogonal metal cutting. Transactions of the ASME, Journal of Engineering for Industry 1985;107:349–54.
[18] Lin ZC, Lin YY, Liu CR. Effects of thermal load and mechanical load on the residual stress of a machined workpiece. International Journal of Mechanical Sciences 1991;33(4):263–78.
[19] Lin ZC, Lai WL, Lin HY, Liu CR. Residual stress with different tool flank wear lengths in the ultra-precision machining of Ni-P alloys. Journal of Materials Progress Technology 1997;65:116–26.
[20] Shih AJ. Finite element simulation of orthogonal metal cutting. Transactions of the ASME, Journal of Engineering for Industry 1995;117:84–93.
[21] Obikawa SH, Shirakashi T, Usui E. Application of computational machining method to discontinuous chip formation. Transactions of the ASME, Journal of Manufacture Science and Engineering 1997;119:667–74.
[22] Guo YB, Dornfeld DA. Finite element analysis of drilling burr minimization with a backup material. Transactions of NAMRI/SME 1998;XXVI:207–11.
[23] Hibbit K, Sorenson, Inc., 1996, ABAQUS/Explicit User's Manual, ver.5.6, Providence, RI.
[24] Kattus JR. Aerospace structural metals handbook, 1975.
[25] Guo YB, Dornfeld DA. Finite element modeling of drilling burr formation process. ASME Transactions, Journal of Manufacture Science and Engineering, in press.
[26] Huang JM, Black JT. An evaluation of chip separation criteria for the FEM simulation of machining. ASME Transactions Journal of Manufacture Science and Engineering 1996;118:545–53.
[27] Iwata K, Osakada K, Terasaka Y. Process modeling of orthogonal cutting by the rigid–plastic finite element method. ASME Transactions, Journal of Engineering Material and Technology 1984;106:132–8.
[28] Shirakashi T, Usui E. Simulation analysis of orthogonal metal cutting mechanism. Proceedings of the International Conference. Production Engineering, Tokyo, Part 1, 1974, p. 535–40.
[29] Hsu HC. An elasto-viscoplastic finite element model of orthogonal metal cutting for residual stress prediction. PhD Dissertation, N.C. State University, 1992.
[30] Kronenberg. Machining science and application, Oxford: Pergamon Press, 1966.